AIChE

Heat and Mass Transfer in Calcination of Limestone Particles

Sirpa Takkinen
Dept. of Energy and Environmental Technology, Lappeenranta University of Technology, FI-53851 Lappeenranta, Finland

Jaakko Saastamoinen
VTT Technical Research Centre of Finland, 40101 Jyväskylä, Finland

Timo Hyppänen
Dept. of Energy and Environmental Technology, Lappeenranta University of Technology, FI-53851 Lappeenranta, Finland

DOI 10.1002/aic.12774
Published online October 20, 2011 in Wiley Online Library (wileyonlinelibrary.com).

The heat and mass-transfer phenomena occurring during the calcination of limestone particles was studied by means of modeling. The applicability of two modeling methods for calcination was compared under different conditions. An unsteady numerical particle model with mass, momentum, energy balance, and shrinking core models were chosen for the study. The influence of different phenomena (chemical kinetics, advective and diffusive mass transfer, and heat transfer) in different conditions was evaluated with the aid of dimensionless parameters, and their relative importance was shown in a regime chart. Especially, the significance of advection was studied and its importance in high CO_2 concentration was observed. Local temperatures inside the particle were obtained by solving a dynamic energy balance in each particle layer including calcination reaction energy and conduction heat transfer. Noticeable temperature differences between constant ambient conditions and the particle were observed. © 2011 American Institute of Chemical Engineers *AIChE J,* 58: 2563–2572, 2012
Keywords: mass transfer, mathematical modeling, heat transfer, reaction kinetics, circulating fluidized beds

Introduction

Fossil fuel combustion power plants represent a major source of anthropogenic CO_2 and, thus, much attention has recently been given to clean combustion applications that easily allow carbon capture. Interest toward new fluidized-bed applications has also grown, for example, oxy-fuel combustion circulating fluidized bed (CFB) and carbonate looping combustion have been the focus of several studies.[1–8] In these processes, limestone is used for capturing either SO_2 or CO_2 or both. The main reaction routes for limestone in the applications are calcination, carbonation, and sulfation.

$$CaCO_3 => CaO + CO_2 \qquad \Delta H = +182.1\ \text{kJ/mol} \qquad (1)$$

$$CaO + CO_2 => CaCO_3 \qquad \Delta H = -182.1\ \text{kJ/mol} \qquad (2)$$

$$CaO + SO_2 + 0.5O_2 => CaSO_4 \qquad \Delta H = -481.4\ \text{kJ/mol} \qquad (3)$$

In the new fluidized-bed combustion applications, the process conditions can greatly differ from traditional fluidized-bed combustion. For example, the gas composition in oxy-fuel combustion can be mainly CO_2 and H_2O depending on the flue gas recycling. The different gas composition can affect limestone reactions; in particular, the higher CO_2 concentration can hinder or completely prevent the calcination reaction.

Correspondence concerning this article should be addressed to S. Takkinen at sirpa.takkinen@lut.fi.

Calcination has been studied extensively in the past decades, a review[7] and different models[9–12] have been presented. Large differences between the values of kinetic data exist in the literature. This can be due, for example, to experimental set-up and the nature of the reaction.[7,13] The limiting process in the calcination has also been discussed.[9,11,12,14,15]

All of the reactions associated with limestone in fluidized-bed systems are heterogeneous reactions in porous media. The physical properties of the used limestone have a strong influence on their ability to capture SO_2 or CO_2. For example, structural characteristics, porosity, pore size distribution, and specific surface area of the sorbent that develops during calcination affect sulfation and/or carbonation reactions.[8,10,16,17] The structural changes depend on the ratio of the molar volumes of the solid products and solid reactant when solid products are formed by the reaction. Additionally, sintering can have a major influence on the particle morphology and, thus, the conversion rates. In calcination, sintering is increased by high-temperatures and time, and it is also accelerated by the presence of CO_2, H_2O, and impurities.[8,16]

Because of the importance of the structural characteristics in limestone reactions, particle level models focus on describing the structure of the porous particle and the way it changes during a gas–solid reaction.[18,19] The models can be categorized in three main groups: pore models focusing on the voids in the particle, grain models focusing on the solid phase (grains), and shrinking core models (SCMs) describing the progress of a reaction front through a homogeneous particle. The shrinking unreacted core model is the most

frequently used model for the description of the kinetics of limestone reactions.[14,20,21] However, a comparison study[22] of these structural models (changing grain size model, random pore model, and distributed pore size model) shows that a single model fails to adequately describe the sulfur capture behavior in a wide range of particle sizes.

Typically, a pseudosteady state assumption has been made in the models, but Hu and Scaroni[12] and Khinast et al.[15] have presented unsteady particle models for calcination. Khinast et al.[15] included advection in their mass-transfer model. For their reaction conditions, the rate-determining step shifted between the chemical reaction and particle diffusion resistance. Hu and Scaroni[12] neglected advection in their model and concluded that under the conditions studied, the calcination rate was influenced by heat transfer, mass transfer, and chemical kinetics.

In this work, the accuracy and validity of two modeling methods under different calcination conditions are evaluated. In the modeling work, the calculation accuracy and speed are contradictory challenges. In this study, the aim is to find the optimum method concerning accuracy and speed to simulate those phenomena that define the most important parameters during calcination under different conditions. Fast calculations are required, especially when limestone reactions are analyzed within three-dimensional reactor models in which the particle level reaction models are repeated several times. In this study, a one-dimensional (1-D) numerical particle model (NPM) with mass, momentum, energy balances, and SCMs were chosen to describe and study limestone calcination. The influence of different phenomena (chemical kinetics, advective and diffusive mass transfer and heat transfer) in different conditions is evaluated with the aid of dimensionless parameters.

Additionally, the effect of advection has often been neglected or its importance has not been shown in most of the previous modeling studies. However, in the new applications, the conditions can be such that the advection may have a large effect to the total conversion time. In this work, this effect has been taken into account and its importance in novel conditions has been studied.

In general, the particle models for limestone reactions should include the unsteady solution of mass and energy transport in the time and space domains for a number of species involved in the reactions. In this study, the accuracy and features of alternative models are evaluated considering the calcination reaction as an application. Subsequently, the model can be used in process conditions in which several parallel reactions exist in changing conditions that are typical for new fluidized-bed process applications using limestone reactions. The results of the study will be required when applying a model for analyses of the reaction phenomena or when using a model as a submodel in comprehensive process models.

Modeling Methods

Numerical particle model

Conservation Equations and Boundary Conditions. In this chapter, the developed 1-D model for a porous spherical limestone particle is presented. The model includes the description of dynamic mass and energy transfer inside the particle and is based on a control-volume method. The model describes the spatial and temporal changes both in the physical properties of the particle (density, porosity, thermal conductivity, and heat capacity) and process parameters (temperature, gas concentration, effective diffusivity, and conversion degree). Certain assumptions and simplifications are required:

1. The particle is assumed to be spherical.
2. The boundary and initial conditions are symmetrical and, thus, 1-D analysis is applied.
3. Changes in the shape and size (diameter) of the particle are not considered (fragmentation and attrition do not occur).
4. Each gas species and the gas mixture follow the equation of state for an ideal gas.
5. A common value of effective diffusivity has been assumed for all the gaseous species.

In practice, the greatest source of error is due to the third assumption, as some limestone may undergo severe fragmentation during calcination. The first two assumptions may also contain error because the particles have varying shapes and may be nonhomogeneous material. In practical cases, the main uncertainties may often lie in the diffusion and reaction parameters.

In the control-volume method, the conservation statement is applied in an integral form to be applicable to a region in space (control volume). This integral form of the conservation statement is usually well-known from the first principles, or it can, in most cases, be developed from the partial differential equation (PDE) form of the conservation law.[23] The conservation equation of mass is written as follows

$$\frac{d}{dt}\int_V \varepsilon_g\ \rho_g\ dV = -\oint_A \left[\varepsilon_g\ \rho_g\ \mathbf{v}\ \right]\cdot \mathbf{n}\ dA + \int_V \sum_i v_i S_i dV. \quad (4)$$

The conservation of mass and momentum is used for solving gas velocity and pressure. Darcy's law for porous media is applied to the momentum equation, giving the following velocity and pressure relation

$$v = -\frac{\kappa}{\mu}\nabla P. \quad (5)$$

In this work, the effect of the porous structure on the pressure drop and the effect of pressure changes to reactions were assumed to be negligible. Thus, the results were not sensitive for the permeability value used in the calculations. The permeabilities of solid product layer may differ significantly.[24] The constant value 10^{-10} m^2 was used for permeability. Dynamic viscosity of gas components is calculated by polynomial fit. The gas mixture's dynamic viscosity is computed as a mass fraction average of the pure species' dynamic viscosity.

The conservation equation of a chemical species is written as follows

$$\frac{d}{dt}\int_V \varepsilon_g\ \rho_g\ Y_i\ dV = -\oint_A \left[\varepsilon_g\ \rho_g\ \mathbf{v}\ Y_i - \varepsilon_g\ \rho_g\ D_{eff}\ \nabla Y_i\right]\cdot \mathbf{n}\ dA + \int_V v_i S_i dV \quad (6)$$

where the first term at the right accounts for the advection and the second for the diffusion. Fluxes of solid species are assumed to be zero. Two gas species are considered: CO_2 and N_2, and two solids: CaO and $CaCO_3$. The local volume fraction of solids

and gas changes according to the relation of molar volume of solid products and reactants and initial porosity

$$\varepsilon_g = \varepsilon_{g,0} - (Z-1)\cdot(1-\varepsilon_{g,0})\cdot X(r,t) \tag{7}$$

$$Z = \frac{V_{M,CaO}}{V_{M,CaCO_3}} \tag{8}$$

$$\varepsilon_s = 1 - \varepsilon_g. \tag{9}$$

The conservation equation of energy is written as follows

$$\frac{d}{dt}\int_V \rho_{tot}\, c_p T\, dV = \oint_A [k_{eff}\,\nabla T]\cdot \mathbf{n}\, dA + \int_V \Delta H S_m dV. \tag{10}$$

Here, only the reaction enthalpy and thermal conduction are considered to be significant terms in the energy equation. The effect of advection was not included in the calculation of heat transfer due to a small Peclet number for heat transfer. Simple equations are used for specific heat capacity of gas components[25] and heat capacities for solids.[26] The gas or solid mixture's heat capacity is computed as a mass fraction average of the different individual species' heat capacities. For a multiphase mixture, the total enthalpy is shown in Eq. 11

$$\begin{aligned} H = \sum m_i h_i &= m_s h_s + m_g h_g \\ &= m_s c_{p,s}(T - T_0) + m_g c_{p,g}(T - T_0) \end{aligned} \tag{11}$$

Polynomial fits are used for gas conductivities.[25] The gas mixture's thermal conductivity is computed as a mass fraction average of the different individual species' conductivity. The thermal conductivity of the solid mixture was obtained from the work of Hu and Scaroni.[12] The effective thermal conductivity for the particle is calculated as the volume average of the gas and the solid properties

$$k_{eff} = \varepsilon_s k_s + \varepsilon_g k_g. \tag{12}$$

The spherical symmetry of the particle implies that the fluxes of heat and the species are equal to zero at the center of particle

$$\text{at } r = 0, \quad \frac{dY_i}{dr} = 0 \tag{13}$$

$$\text{at } r = 0, \quad \frac{dT}{dr} = 0. \tag{14}$$

The fluxes of energy and species are defined by the external conditions at the surface of the particle, the boundary conditions for which are as follows

$$-\oint_A \left[\varepsilon_g\, \rho_g\, \mathbf{v}\, Y_i - \varepsilon_g\, \rho_g\, D_{eff}\, \nabla Y_i\right]\cdot \mathbf{n}\, dA = \rho_g k_f \left(Y_{i,\infty} - Y_{i,s}\right) A$$

$$\text{at } r = R \tag{15}$$

$$\oint_A [k_{eff}\,\nabla T]\cdot \mathbf{n}\, dA = h(T_\infty - T_s)A + \varepsilon\sigma\left(T_\infty^4 - T_s^4\right)A$$

$$\text{at } r = R. \tag{16}$$

The external mass and heat-transfer coefficients were calculated in this study assuming a stagnant gas environment using value two for the Sherwood and Nusselt numbers "Sh and Nu." The values of the source terms for mass and heat balance are obtained via the relations for the chemical reaction kinetics. In the studied case, only the calcination reaction (Eq. 1) was considered in the modeling.

Numerical Solution Technique and Computational Procedure. The temperature and gas concentrations were initially constant along the radius of the limestone particle. The values of the other parameters (such as porosity) were also initially constant along the particle radius. The control-volume numerical method was used for solving the system of the conservation equations (Eqs. 4, 6, and 10) for obtaining the values of temperatures and gas concentrations along the limestone particle radius and their change in time. For numerical purposes, the spherical particle was divided into a sufficient amount of spherical concentric computational cells of equal radial thickness. In most of the studied cases, 10 computational cells were used. The selected number of cells was based on the comparison studies with much larger number of cells. Boundary conditions for the center and surface were given by a ghost cell and a numerical grid. The conservation equations were discretized for each cell. The diffusion term was approximated using a first-order scheme. The time dependence of the gas species' equation was modeled with an implicit method to allow stable calculations with larger time steps that were needed for faster simulations. Tridiagonal matrix algorithm (TDMA)-method was used to solve a tridiagonal system of linear algebraic equations. The 1-D control-volume approach was compared with the CFD analysis in which the same phenomena and the same submodels were considered for verifying the 1-D model. The CFD solver ANSYS-FLUENT was used to solve the governing equations, including the conservation of mass, momentum, energy, and species. The model results were in agreement and the correctness of the particle model could be verified.

Shrinking core model

The SCM without advection has been applied elsewhere.[14] The pseudosteady state mass balance for a spherical shell is

$$\begin{aligned} &-4\pi R^2\left(D\frac{dP_{CO_2}}{dR}\right)_R + 4\pi(R+\Delta R)^2\left(D\frac{dP_{CO_2}}{dR}\right)_{R+\Delta R} \\ &+ 4\pi R^2 (vP_{CO_2})_R - 4\pi(R+\Delta R)^2 (vP_{CO_2})_{R+\Delta R} = 0 \end{aligned} \tag{17}$$

where the two first terms are due to diffusion and the two last due to advection. When $\Delta R \to 0$, we get

$$\frac{d}{dR}\left(DR^2\frac{dP_{CO_2}}{dR} - vR^2 P_{CO_2}\right) = 0 \tag{18}$$

The boundary condition for the receding core is

$$-\frac{\Delta\rho R_g T}{M_{CO_2}}\frac{dR_c}{dt} = -D\left(\frac{dP_{CO_2}}{dR}\right)_{R=R_c} + (vP_{CO_2})_{R=R_c} \tag{19}$$

The term on the left hand side describes the flux generated at the reaction front. The first term on the right hand side is the flux due to diffusion and the second due to advection. The reaction front recedes due to reaction by

$$\frac{dR_c}{dt} = -k_c V_{MCaO} f(P_{CO_2}) \tag{20}$$

The calcination temperature (on the shrinking core) was calculated from the simple thermal balance considering that

Table 1. Values of Variables in the Base Case Calculations

Particle diameter (μm)	100, 500, 1000
Initial sorbent particle voidage ε_g (–)	0.3
Temperature (K)	1123
Pressure (Pa)	101,325
Gas atmosphere (outside particle)	100 vol % N_2, 0 vol % CO_2

the heat transfer by radiation and convection to the surface is equal to the conduction through two concentric spherical surfaces (particle surface and shrinking core). This heat flux is equal to the heat flux required for calcination.

Results and Discussion

Evaluation of calculation parameters

The kinetic and reactivity parameters are obtained from the work of Garcia-Labiano et al.[14] The kinetic parameters of Mequinenza limestone were used. The reaction rate is defined by the following equation

$$r_c = k_c \cdot S_e \cdot f(CO_2) = k_c \cdot S_e \cdot \left(1 - \frac{P_{CO_2}}{P_{eq}}\right). \quad (21)$$

The molecular diffusivity is estimated with the following equation

$$D_{CO_2} = 0.000161 \cdot (T/1100)^{1.75} \cdot (101,325/P_{tot}). \quad (22)$$

The equations of Knudsen and the effective diffusion are obtained from the work of Garcia-Labiano et al.[14]

Dimensionless parameters

The relative effect of each of the processes (chemical kinetics and advective and diffusive mass transport) can be analyzed by dimensionless parameters. The dimensionless parameters can be formed at least in three ways. The traditional way is to perform a dimensional analysis of the system, in which all of the affecting variables of the system are collected and their dimensions are analyzed. Another way is to form dimensionless parameters from physical models, which are described with mathematical differential equations. The relative difference of various terms can be estimated based on dimensionless numbers appearing during nondimensionalizing. The third way is to specify dimensionless parameters as ratios of different quantities: for example, a ratio of forces. This is a physical interpretation of the system and is more suitable when the system is complex and time-dependent. In this case, the evaluation of dimensionless parameters is made with the physical interpretation of the quantities because the different models are compared, and there are several interdependent parameters.

The ratio of chemical kinetics and diffusion is characterized by the Thiele modulus. The Thiele modulus is a nondimensional ratio of the two time scales involved in the heterogeneous system, the time scale for diffusion L_c^2/D to the reaction time scale

$$\Phi_m = L_c \left(\frac{S_{CO_2}}{\varepsilon_g \rho_g D_{eff}}\right)^{1/2} \quad (23)$$

It is generally known that if the intraparticle diffusion is the controlling mechanism (Thiele $>> 1$), then the sharp interface SCM can be used. However, if the kinetics are the controlling mechanism (Thiele $<< 1$), then the SCM is no longer applicable and the uniform particle model can be used. When the reaction kinetics and diffusion ($0.1 <$ Thiele < 10) both have an effect, they should both be taken into account simultaneously in the modeling.

The significance of advection can be judged by Peclet numbers. The Peclet mass-transfer number describes the ratio of advective and diffusive mass transfers

$$Pe_m = \frac{L_c v_g}{D_{eff}} \quad (24)$$

In the conditions of very low Peclet numbers (Pe $<< 1$), we obtain a diffusion-limited mass transfer. In contrast, when the Peclet number is large (Pe $>> 1$), the effect of diffusion is almost negligible.

The ratio of chemical kinetics and thermal diffusion is characterized by the Thiele heat-transfer modulus

$$\Phi_h = L_c \left(\frac{S_{CO_2}}{\rho_g \alpha}\right)^{1/2} \quad (25)$$

Even though the definitions of dimensionless numbers are well established, there has been little discussion concerning the role of understanding the limitations of phenomena locally in the particle. Understanding the local effects is important from a fundamental standpoint because an average value represents a composite of the distribution of the local phenomena. For example, the limiting process of the reaction can change in time and in space, which should be recognized for more accurate analysis of the reactions. The average value can mislead the interpretation of the results because it can underestimate or overestimate the limiting phenomena, and it does not necessarily describe the phenomena in the reaction front. This is especially important when different models are compared. Additionally, there is no unambiguous method to define the average values of dimensionless numbers in these cases for which the limitation changes in time and space. In this study, the average diffusion coefficient of the particle applied in dimensionless numbers is estimated based on the mass-transfer resistance in the middle of the particle, and the velocity is estimated based on the velocity in the outermost element.

Base case calculations with the NPM

The results from NPM without the energy equation were compared with the results of Garcia-Labiano et al.[14] under atmospheric pressure for Mequinenza limestone at a temperature of 1123 K for a particle size of 0.8–1 mm in different CO_2 concentrations. The particle model results were in agreement.

The base case computations were first carried out assuming the set of input parameters reported in Table 1. Figure 1 shows the conversion for each particle size in the base case computations with the NPM. As expected, the calcination time increases with increasing particle size. The calcination times for different particle sizes approximately correspond with the measured calcination times in the literature.[12,14,27] For small particles ($\sim$10 μm), the calcination time is approximately only a few seconds, whereas the calcination of larger particles ($\sim$1 mm), as used in bubbling fluidized-bed applications, can require 5–15 min.

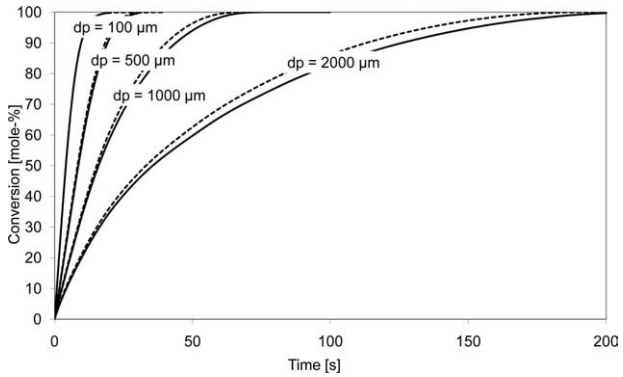

Figure 1. Conversion times for different particle sizes (solid line—diffusion; dashed line—diffusion and advection).

Figure 2 presents the extent of calcination at different radial positions at different total conversion levels for each particle size. Different reaction zone types can be noticed in the different particle size cases. Decomposition of the largest particle took place at a definite boundary between the CaO and $CaCO_3$ phases. Calcination occurred with different conversion levels at different locations in the medium-sized particle. The conversion profile of the smallest particle is uniform throughout the particle at different conversion stages. The effect of diffusion increases when the particle size increases, which is characterized by increasing the Thiele number in Figure 3.

The temperature profile of each particle size is presented in Figure 4. It can be seen that the maximum temperature drop is 35 K (in the 1000 μm particle). The heat-transfer effect increases when the particle size increases, which is characterized by the Thiele heat-transfer number in Figure 3.

Accuracy and validity of the NPM with and without advection

The numerical 1-D particle model was applied to compare the differences between the diffusion and diffusion–advection models to evaluate the error caused by neglecting the advection. The effect of advection was examined in different cases: variation in particle size, temperature, or CO_2 concentration. The dimensionless numbers were used to evaluate when the advection can be neglected.

Effect of Particle Size. The increasing effect of advection when the particle size increases can be seen from the difference between the base case computations with diffusion and diffusion–advection models presented in Figure 1. For example, the difference in conversion times is approximately 9% for the 1000 μm particle. The particle size affects the mass transport phenomena. The effect of advection increases in

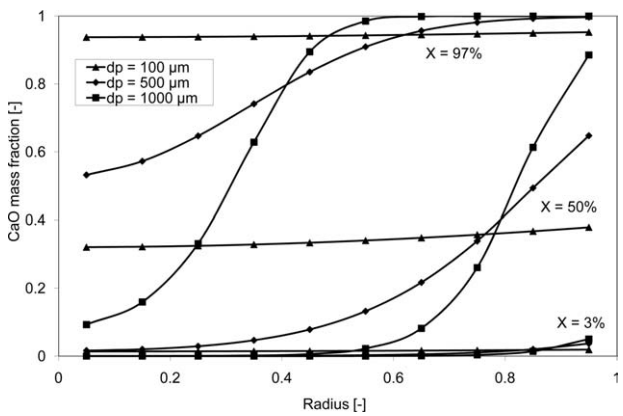

Figure 2. Mass fraction of CaO at different conversion stages (*X*) as a function of radius.

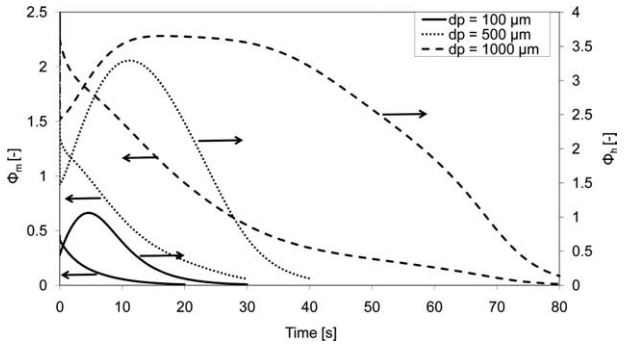

Figure 3. Thiele mass and heat transfer numbers for different particle sizes (diffusion case).

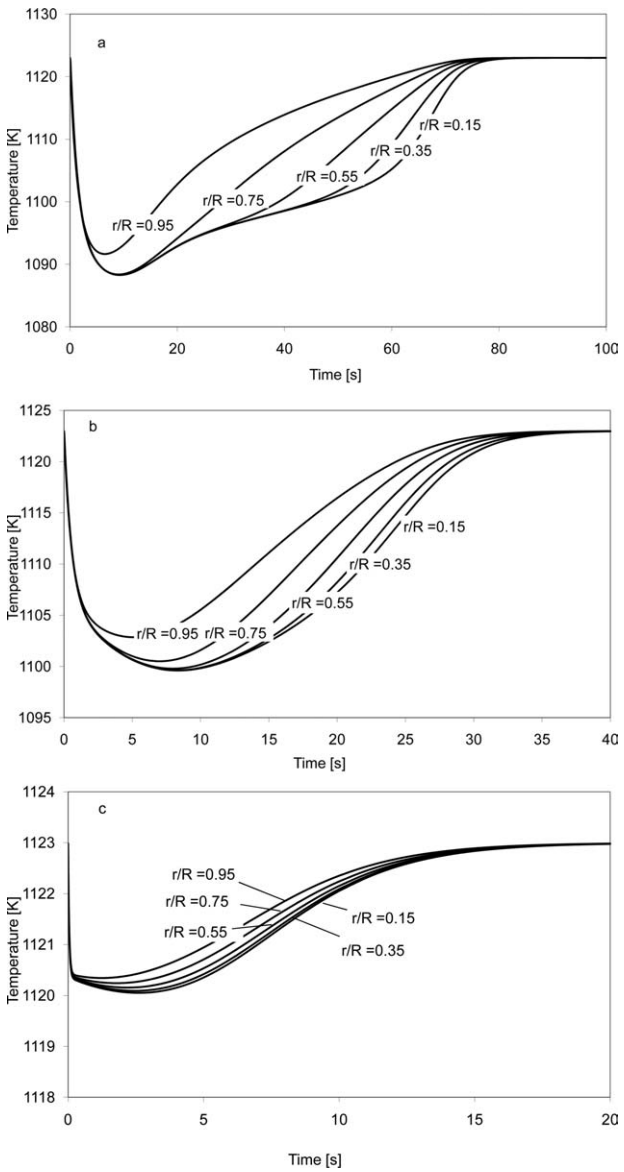

Figure 4. Temperature as a function of time for (a) 1000 μm, (b) 500 μm, and (c) 100 μm particles.

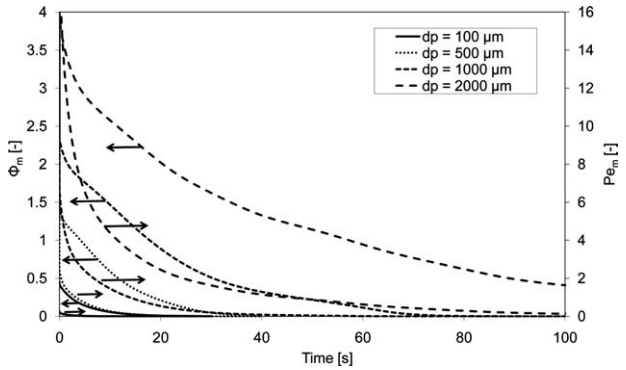

Figure 5. Thiele and Peclet numbers for different particle sizes.

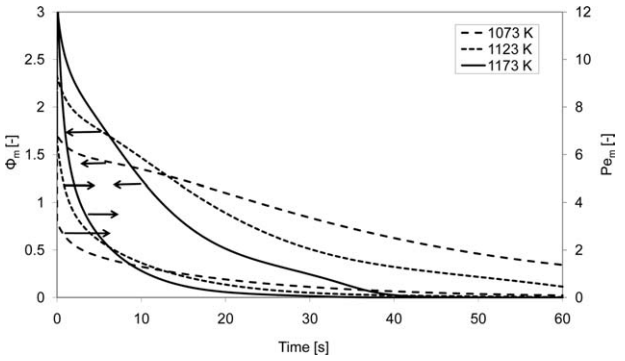

Figure 7. Thiele and Peclet numbers for different temperatures.

relation to diffusion as the particle size increases because the diffusive flow decreases, which can be observed from the Peclet number in Figure 5. Simultaneously, diffusion has also more importance as a limiting process in relation to chemical kinetics, as can be seen from the increasing value of the Thiele number in Figure 5.

Effect of Temperature. Increasing temperature leads to increasing reactivity and decreasing reaction time. Thus, the diffusion flow becomes more limiting. In addition, temperature gradients within the particle increase due to higher reaction rates and, thus, the role of heat transfer becomes more dominating. The absolute conversion time is almost the same for all the temperatures between the diffusion and diffusion–advection models, as can be seen from Figure 6. However, the relative difference and the relative error in the diffusion calculation are larger for higher temperatures. The temperature increase affects the kinetics, and simultaneously, the reactivity and gas velocity increase, consequently increasing the Pe_m and Thiele numbers, which can be observed in Figure 7.

Effect of CO_2 Concentration. The increasing CO_2 concentration leads to decreasing reactivity and, thus, the reaction time increases. Figure 8 presents the difference between diffusion and diffusion–advection models in different CO_2 concentrations. It can be seen that the difference between the models increases as the CO_2 concentration increases. This cannot be clearly explained by the Pe_m number, as shown in Figure 9 presenting the values for Thiele and Pe_m at 0, 10, and 30 vol % calculated with the diffusion–advection model.

The increase in CO_2 concentration affects both the kinetics and mass transport. The effect on kinetics originates from the source term via the difference in the equilibrium decomposition pressure and the CO_2 partial pressure inside the particle and, thus, the reactivity decreases as the CO_2 concentration increases. At the same time, the mass transport phenomenon is dependent on the difference of the CO_2 partial pressure inside and outside the particle, and because this difference is smaller for high CO_2 concentrations, the diffusion flow is smaller. If the CO_2 difference is not taken into account in the dimensionless numbers, as in Eqs. 23 and 24, the numbers are not able to explain the advection flow effect, as can be seen from Figure 9. However, the CO_2 concentration could be considered in dimensionless variables by comparing the magnitudes of the diffusive, reactive, and convective terms in Eq. 6. Thus, one may make the following deductions that define the modified dimensionless Thiele and Peclet numbers, as in Eqs. 26 and 27. Thus, the dimensionless numbers are able to explain the increasing difference between the diffusion and diffusion–advection results, as can be seen from Figure 10.

$$\Phi_m^2 = \frac{\text{Reactions}}{\text{Diffusion}} \approx \frac{S_{CO_2} V}{\varepsilon_g \rho_g D_{eff} \nabla Y_i \Delta A} \approx \frac{S_{CO_2} V}{\varepsilon_g \rho_g D_{eff} \frac{\Delta Y_i}{L_c} A} \approx \frac{S_{CO_2} L_c^2}{\varepsilon_g \rho_g D_{eff} \left(Y_{eq} - Y_{CO_2,g}\right)} \tag{26}$$

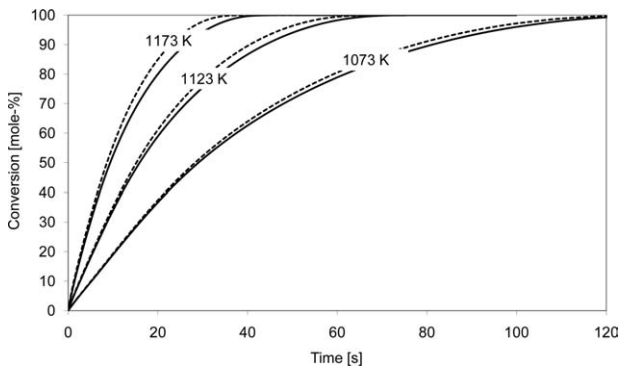

Figure 6. Difference between diffusion and diffusion–advection models at different temperatures (solid line—diffusion; dashed line—diffusion and advection).

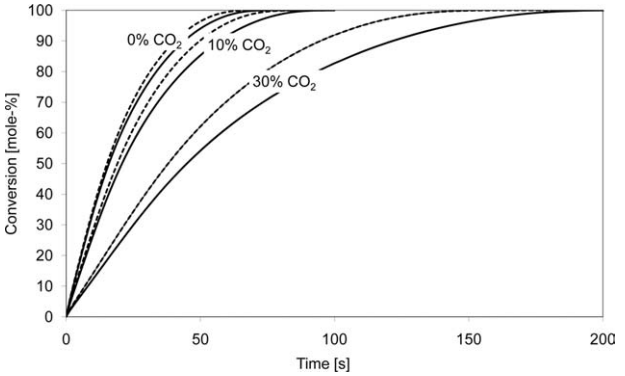

Figure 8. Difference between diffusion and diffusion–advection models at different CO_2 concentrations (solid line—diffusion; dashed line—diffusion and advection).

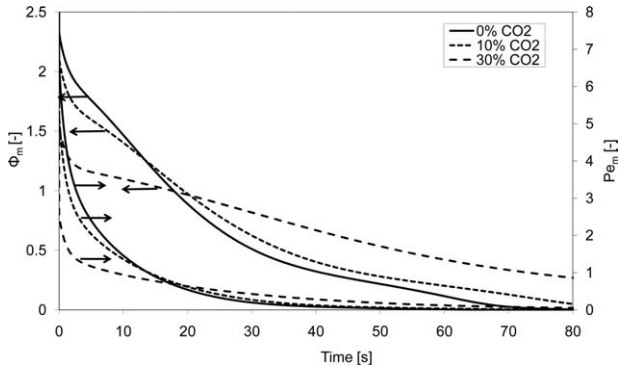

Figure 9. Thiele and Peclet numbers for different CO_2 concentrations.

$$\mathrm{Pe_m} = \frac{\text{Advection}}{\text{Diffusion}} \approx \frac{\varepsilon_g \rho_g v_g Y_i}{\varepsilon_g \rho_g D_{\text{eff}} \nabla Y_i} = \frac{v_g Y_i}{D_{\text{eff}} \nabla Y_i} \approx \frac{v_g Y_i}{D_{\text{eff}} \frac{\Delta Y_i}{L_c}} \approx \frac{L_c v_g Y_{\text{eq}}}{D_{\text{eff}} \left(Y_{\text{eq}} - Y_{\text{CO}_2,\text{g}}\right)} \quad (27)$$

Accuracy and validity of the SCM

The NPM and SCM are compared to evaluate the validity area of the SCM. The SCM is obtained in the limiting case when the chemical reaction rate coefficient approaches infinity (now labeled as SCM 2). In this case, the front will be at the chemical equilibrium. A more exact approach is to apply an apparent chemical reaction at the front (now labeled as SCM 1). The apparent reaction rate with respect to the area of the shrinking core can be related to the intrinsic reactivity (see, e.g., Shimizu et al.[28]). The reaction rate is obtained by the effectiveness factor for a large Thiele modulus. In the present case, the method is ambiguous because the chemical reactivity and diffusivity depend on the conversion. Here, the reaction rate coefficient is calculated using values at 50% conversion. It is also possible to optimize the reaction rate coefficient at the front based on measurements or more comprehensive calculations. However, in this case, the result depends on a range of parameters (ambient temperature, concentration, and particle size).

The difference between the different models is presented in Table 2. Both SCMs give much smaller conversion times than the NPM with the smallest particle size. When the particle size is increased, SCM 1 gives results with modest differences compared with the NPM. This result corresponds to the general knowledge that the SCM is valid with larger Thiele numbers when the diffusion limitation increases. However, the difference increases when the particle size is further increased (up to 2000 μm). This can be due to the large partial pressure of CO_2 generated inside the particle. Simultaneously, the temperature decreases inside the particle due to the reaction and, thus, the CO_2 pressure can be close to the equilibrium decomposition pressure and cause the increased difference. Meanwhile, SCM 2 gives much smaller conversion times than the other two models at all particle sizes, although the difference decreases when the particle size and diffusion limitation increases.

Table 2. Difference Between the Different Models

			Difference (%)			
			NPM*-SCM 1†		NPM*-SCM 2‡	
d_p (μm)	T (K)	CO_2 (vol %)	Diffusion	Diffusion–Advection	Diffusion	Diffusion–Advection
100	1123	0	81.2	81.2	97.0	97.0
500	1123	0	15.6	12.7	68.5	67.8
1000	1123	0	3.9	−3.4	52.9	50.1
2000	1123	0	10.7	2.2	45.4	41.0
1000	1173	0	−9.2	−23.2	40.7	34.1
1000	1073	0	16.7	13.1	64.2	63.1
1000	1123	10	−14.4	−11.5	35.6	37.6
1000	1123	30	−66.9	−28.3	−8.6	16.7

*Numerical particle model.
†Shrinking core model with apparent reaction rate coefficient.
‡Shrinking core model with infinite reaction rate.

The difference between NPM and SCM 1 increases when the temperature is either decreased or increased. The results of SCM 2 show decreasing differences with increasing temperature, which can be explained by the increasing Thiele number. The difference between SCM 1 and NPM also increases when the CO_2 concentration is increased in the surrounding gas. The conversion times of SCM 1 are much longer; this can be due to the high CO_2 concentration that is close to the equilibrium decomposition pressure. Therefore, even small differences in CO_2 concentration can lead to a large error. The effect of CO_2 concentration is opposite for SCM 2; the difference decreases with increasing CO_2 concentration.

The advection calculations correspond well with the diffusion model calculations; the difference between SCM 1 and NPM is highest with the smallest particle size and modest with the larger particles. In the case of SCM 2, a large difference is obtained with all the particle sizes. As with the diffusion model calculations, the difference between NPM and SCM 1 increases when the temperature is either decreased or increased. As with the diffusion models, the CO_2 concentration increase creates larger differences with SCM 1 and smaller differences with SCM 2. In general, the effect of advection is similar within the SCMs than with the NPM; the effect of advection increases when the particle size, temperature, or CO_2 concentration increases. The difference is most obvious for high CO_2 concentrations.

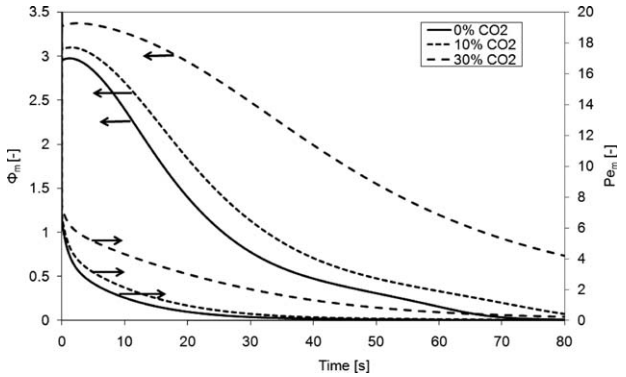

Figure 10. Modified Thiele and Peclet numbers for different CO_2 concentrations.

Summary of the reaction and mass-transfer limitations

The regimes of the calcination reaction in porous limestone particles are presented in Figure 11. The regions in which the calcination is controlled either by diffusion or chemical kinetics or enhanced by advection are shown with labels, and the mixed regimes of different combinations of

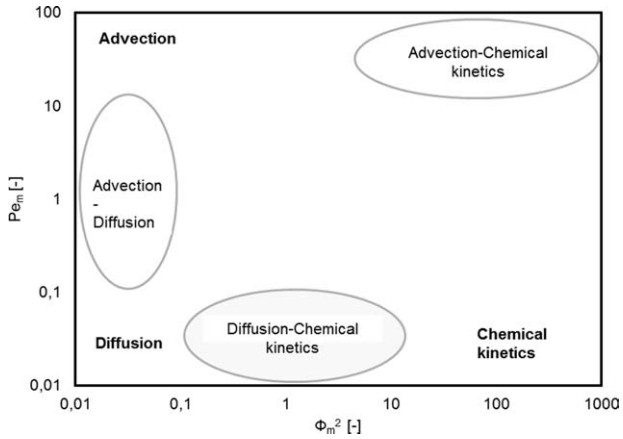

Figure 11. Regime diagram for advection, diffusion, and chemical kinetics reproduced from the work of Lopes et al.[29]

the limitation regimes are shown in circled areas. The regime diagram is reproduced from the work of Lopes et al.[29]

In the present study, the ratio of Thiele and Peclet number in the investigated cases is almost constant as can be seen from Figure 12. This can be explained by noticing that advection flow is mainly produced from the gas production due to reactions. Thus, the advection flow is proportional to reactions, and as a consequence, Thiele and Peclet numbers are closely linked. The data points present time averages of modified Thiele and Peclet numbers for each diffusion–advection case calculated with the NPM. In calcination, the reactions can be concentrated in a narrow zone inside the particle resulting in the progression of a steep conversion profile and a nonlinear reaction–diffusion problem. The Thiele modulus and Peclet number are usually defined for a process with uniform diffusivity and rate coefficient. Because of nonlinearity, average dimensionless parameters are applied. In Figure 12, the difference between the diffusion and diffusion–advection cases calculated with the NPM is presented. Most cases are in the area of dominating advection and kinetics. Only the smallest particle size case is in the regime where the chemical kinetics is a limiting mechanism. In that regime, the diffusion model leads to an accurate solution. As data points move toward the dominating regime of advection and kinetics, the role of advection

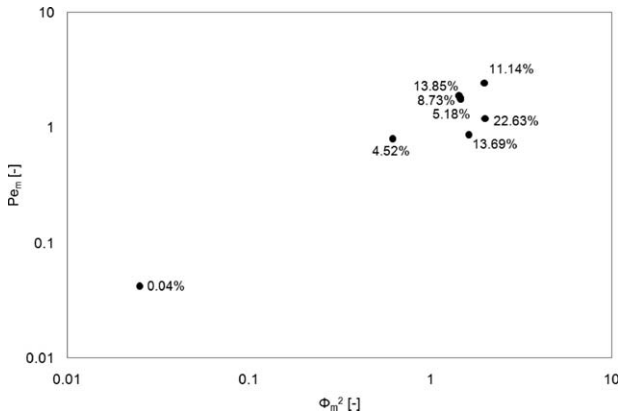

Figure 12. Regime chart with data points of the investigated cases and difference in these cases between diffusion and diffusion–advection models.

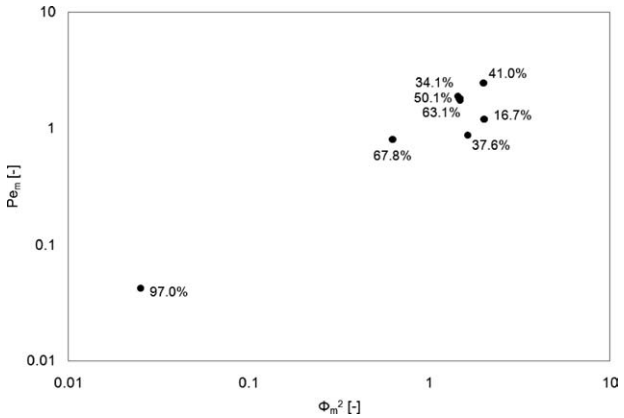

Figure 13. Difference between the NPM and SCM 2 at different data points.

increases. The diffusion model is not able to consider the advective portion of the flow, and the difference shows an increasing trend. Other heterogeneous reactions and processes can have a larger variation of regime points, and a similar chart can be used when the importance of different phenomena is evaluated.

The difference between the NPM and SCM 2 is presented in the regime diagram at different data points in Figure 13, and the difference between NPM and SCM 1 is presented in a similar chart in Figure 14. In the SCM 2 model, the infinite reaction rate is applied and, thus, a diffusion limitation is assumed. Therefore, the difference is greatest with small Thiele and Peclet numbers and decreases in the other regimes; however, the difference is relatively large in the whole regime area. When the apparent reaction order is used, the difference between the NPM and the SCM is smaller throughout the regime area, but there is no consistent explanation for the difference between the models in different points. Only the largest difference with the smallest particle size case can be explained with the small Thiele number.

Conclusions

The heat and mass-transfer phenomena occurring during the calcination of limestone particles were studied by means of modeling. Intraparticle advection has been neglected in the majority of reaction–diffusion studies in limestone particles conducted to date. However, this transport mechanism

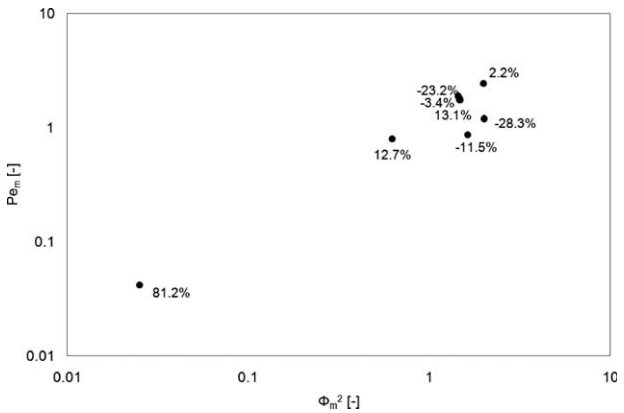

Figure 14. Difference between the NPM and SCM 1 at different data points.

can contribute significantly to the total intraparticle transport rate. Neglecting advection in the NPM will create larger errors for conditions that are typical for smaller diffusion or higher reactivities, as found for larger particles and higher temperatures. Especially large differences were found for high CO_2 concentrations of the environment, in which case, the diffusion flow was reduced.

The increasing difference is due to the increased ratio of advection flow to diffusion flow, which is described by the Pe_m number. However, the definition of Pe_m does not consider the reduced diffusion flow due to the increased CO_2 of the environment, and consequently, it cannot be used as the criterion for analyzing the error of neglecting advection flow. However, if the CO_2 difference is considered in the Thiele and Peclet numbers, the numbers are able to evaluate the validity of the model at high CO_2 concentrations. The effect of advection can be evaluated with the aid of regime chart in different cases.

The applicability study of the SCMs showed that the model with an infinite reaction rate produces large differences compared with the NPM through the studied regime. The difference is diminished when the model with an apparent reaction rate is applied; however, there always exists a certain difference between the two models. This difference is emphasized with small particle sizes or when the CO_2 concentration is high in the surrounding gas.

In these studies, the effect of heat transfer was also considered. A noticeable temperature drop with respect to ambient was detected when the particle size was greater or the temperature was higher. This temperature drop changes during calcination with maximum close to the beginning of calcination. It has also a notable effect increasing the calcination time. The particle temperature itself was rather uniform with maximum temperature differences inside the particle in the studied cases around 20–30 K.

The absolute values for different parameters in different models should be compared with caution, for example, the effect of advection might be included in the diffusion term if the experimental results have been analyzed by a method without advection. Calcination and limestone reactions are the focus of several novel applications, such as carbonate looping combustion and oxyfuel (CFB) combustion. In this study, high CO_2 concentration, which also exists in the new applications, was shown to have significant effect in the modeling. Therefore, the observations of this study should be taken into account when modeling the new applications. A significant feature of the presented 1-D unsteady numerical model including advection is its capability to consider an arbitrarily changing environment. That feature was not used in this study, but it will be required when analyzing the novel applications.

Acknowledgments

Sirpa Takkinen is grateful for the scholarship from the Graduate School of Energy Technology. This work was supported by the Academy of Finland under Grant Nos. 124368 and 123938.

Notation

A = area, m^2
c_p = specific heat capacity, J/(kg K)
d_p = diameter of the particle, m
D = diffusion coefficient, m^2/s
h = convection heat-transfer coefficient, W/(m^2 K) and enthalpy, J/kg
ΔH = reaction enthalpy, J/mol
k = thermal conductivity, W/mK
k_c = chemical reaction rate constant, mol/(m^2 s)
k_f = mass-transfer coefficient, m/s
L_c = characteristic length, m ($V/A = R/3$ for a sphere)
m = mass, kg
M = molecular weight, kg/mol
Nu = Nusselt number = hL/k_f [-]
P = pressure, Pa
Pe = Peclet number [-]
r = radial coordinate within the particle, m
r_c = reaction rate of calcinations, mol/(m^3 s)
R = radius of the particle, m
R_g = ideal gas constant, J/(mol K)
S = source/sink, kg/(m^3 s)
S_e = specific surface area, m^2/m^3
Sh = Sherwood number = kL/D [-]
t = time, s
T = temperature, K
v = velocity, m/s
V = volume, m^3
V_M = molar volume, m^3/mol
X = conversion [-]
Z = stoichiometric volume ratio of solid product to solid reactant [-]
Y = mass fraction of species [-]

Greek letters

α = thermal diffusivity $\alpha = k_{eff}/\rho c_p$, m^2/s
ε = volume fraction, emissivity [-]
κ = permeability, m^2
μ = dynamic viscosity, kg/(m s)
ρ = density, kg/m^3
$\Delta\rho$ = density reduction in calcinations, kg/m^3
υ = stoichiometric coefficient [-]
Φ = Thiele modulus [-]
σ = Stefan–Boltzmann constant, W/(m^2 K^4)

Subscripts

∞ = infinite
c = core
eff = effective
eq = equilibrium
g = gas
h = heat transfer
i = species i
m = mass, mass transfer
tot = total
s = surface, solid
0 = initial

Literature Cited

1. Abanades JC, Anthony EJ, Lu DY, Salvador C, Alvarez D. Capture of CO_2 from combustion gases in a fluidized bed of CaO. *AIChE J*. 2004;50:1614–1622.
2. Jia L, Tan Y, Wang C, Anthony EJ. Experimental study of oxy-fuel combustion and sulfur capture in a mini-CFBC. *Energy Fuels*. 2007;21:3160–3164.
3. Jia L, Tan Y, Anthony EJ. Emissions of SO_2 and NO_x during oxy-fuel CFB combustion tests in a mini-circulating fluidized bed combustion reactor. *Energy Fuels*. 2010;24:910–915.
4. Myöhänen K, Hyppänen T, Pikkarainen T, Eriksson T, Hotta A. Near zero CO_2 emissions in coal firing with oxyfuel CFB boiler. *Chem Eng Technol*. 2009;32:355–363.
5. Nsakala N, Liljedahl GN, Turek DG. *Commercialization Development of Oxygen Fired CFB for Greenhouse Gas Control* (PPL Report No. PPL-07-CT-20). Pittsburgh: U.S. Department of Energy, 2007:76–89.
6. Shimizu T, Hirama T, Hosoda H, Kitano K, Inagaki M, Tejima K. A twin fluid-bed reactor for removal of CO_2 from combustion processes. *Trans IChemE*. 1999;77(Part A):62–68.
7. Stanmore BR, Gilot P. Review—calcination and carbonation of limestone during thermal cycling for CO_2 sequestration. *Fuel Process Technol*. 2005;86:1707–1743.
8. Symonds RT, Lu DY, Macchi A, Hughes RW, Anthony EJ. CO_2 capture from syngas via cyclic carbonation/calcination for a

naturally occurring limestone: modelling and bench-scale testing. *Chem Eng Sci*. 2009;64:3536–3543.
9. Dennis JS, Hayhurst AN. *The calcination of limestones particles in fluidized beds*. In: Østergaard K, Sørensen A, editors. *Proceedings of the Fifth Engineering Foundation Conference on Fluidization*. New York: Engineering Foundation, 1986:563–570.
10. Fierro V, Adánez J, Garcia-Labiano F. Effect of pore geometry on the sintering of Ca-based sorbents during calcination at high temperatures. *Fuel*. 2004;83:1733–1742.
11. Hills AWD. The mechanism of the thermal decomposition of calcium carbonate. *Chem Eng Sci*. 1968;23:297–320.
12. Hu N, Scaroni AW. Calcination of pulverized limestone particles under furnace injection conditions. *Fuel*. 1996;75:177–186.
13. Blamey J, Anthony EJ, Wang J, Fennell PS. The calcium looping cycle for large-scale CO_2 capture. *Prog Energ Combust*. 2010;36:260–279.
14. Garcia-Labiano F, Abad A, de Diego LF, Gayan P, Adánez J. Calcination of calcium-based sorbents at pressure in a broad range of CO_2 concentrations. *Chem Eng Sci*. 2002;57:2381–2393.
15. Khinast J, Krammer GF, Brunner C, Staudinger G. Decomposition of limestone: the influence of CO_2 and particle size on the reaction rate. *Chem Eng Sci*. 1996;51:623–634.
16. Manovic V, Charland JP, Blamey J, Fennell PS, Lu DY, Anthony EJ. Influence of calcination conditions on carrying capacity of CaO-based sorbent in CO_2 looping cycles. *Fuel*. 2009;88:1893–1900.
17. Zarkanitis S, Sotirchos SV. Pore structure and particle size effect on limestone capacity for SO_2 removal. *AIChE J*. 1989;35:821–830.
18. Sahimi M, Gavalas GR, Tsotsis TT. Statistical and continuum models of fluid–solid reactions in porous media. *Chem Eng Sci*. 1990;45:1443–1502.
19. Ramachandran PA, Doraiswamy LK. Modeling of noncatalytic gas–solid reactions. *AIChE J*. 1982;28:881–900.
20. Silcox GD, Kramlich JC, Pershing DW. A mathematical model for the flash calcination of dispersed $CaCO_3$ and $Ca(OH)_2$ particles. *Ind Eng Chem Res*. 1989;28:155–160.
21. Zevenhoven R, Yrjas P, Hupa M. Sulfur dioxide capture under PFBC conditions: the influence of sorbent particle structure. *Fuel*. 1998;77:285–292.
22. Adánez J, Gayan P, Garcia-Labiano F. Comparison of mechanistic models for the sulfation reaction in a broad range of particle sizes of sorbents. *Ind Eng Chem Res*. 1996;35:2190–2197.
23. Tannehill JC, Anderson DA, Pletcher RH. *Computational Fluid Mechanics and Heat Transfer*, 2nd ed. Philadelphia: Taylor & Francis, 1997:71–76.
24. Lech R. Thermal decomposition of limestone: Part 4—permeability of product layer. *Silicates Industriels*. 2007;72:45–52.
25. Laine J. *Kaasujen ainearvot prosessilaskentaa varten*. Helsinki: Hakapaino Oy, 1998.
26. Green DW, Perry RH. *Perry's Chemical Engineers' Handbook*, 8th ed. New York: McGraw-Hill, 2008.
27. Smith IM. *Properties and Behaviour of SO_2 Adsorbents for CFBC*. London: IEA Clean Coal Centre, 2007.
28. Shimizu T, Peglow M, Yamagiwa K, Tanaka M. Comparison among attrition-reaction models of SO_2 capture by uncalcined limestone under pressurized fluidized bed combustion conditions. *Chem Eng Sci*. 2003;58:3053–3057.
29. Lopes J, Cardoso SSS, Rodrigues AE. Convection, diffusion, and exothermic zero-order reaction in a porous catalyst slab: scaling and perturbation analysis. *AIChE J*. 2009;55:2686–2699.

Manuscript received Mar. 14, 2011, and revision received Aug. 13, 2011.